frontiers in Environmental Chemistry

ORIGINAL RESEARCH
published: 10 August 2021
doi: 10.3389/fenvc.2021.692810

Synthesis, Optical Characterization, and Adsorption of Novel Hexavalent Chromium and Total Chromium Sorbent: A Fabrication of Mulberry Stem Biochar/Mn-Fe Binary Oxide Composite *via* Response Surface Methodology

Shuiping Xu[1,2], *Meina Liang*[1,3]*, *Yanmei Ding*[1], *Dunqiu Wang*[1,3], *Yinian Zhu*[1,3] and *Linbo Han*[2]*

[1]College of Environmental Science and Engineering, Guilin University of Technology, Guilin, China, [2]College of Health Science and Environmental Engineering, Shenzhen Technology University, Shenzhen, China, [3]Guangxi Collaborative Innovation Center for Water Pollution Control and Water Safety in Karst Area, Guilin University of Technology, Guilin, China

OPEN ACCESS

Edited by:
Andrew R Zimmerman,
University of Florida, United States

Reviewed by:
Xiangke Wang,
North China Electric Power University, China
Saba Yavari,
University of Technology Petronas, Malaysia
Amin Mojiri,
Hiroshima University, Japan

***Correspondence:**
Meina Liang
liangmeinaa@163.com
Linbo Han
hanlinbo@sztu.edu.cn

Specialty section:
This article was submitted to Sorption Technologies, a section of the journal Frontiers in Environmental Chemistry

Received: 06 May 2021
Accepted: 30 June 2021
Published: 10 August 2021

Citation:
Xu S, Liang M, Ding Y, Wang D, Zhu Y and Han L (2021) Synthesis, Optical Characterization, and Adsorption of Novel Hexavalent Chromium and Total Chromium Sorbent: A Fabrication of Mulberry Stem Biochar/Mn-Fe Binary Oxide Composite via Response Surface Methodology. Front. Environ. Chem. 2:692810. doi: 10.3389/fenvc.2021.692810

In this study, a new generation chromium sorbent, mulberry stem biochar/Mn-Fe binary oxide composite (MBC-MFC), was fabricated by chemical precipitation on carbonized mulberry stem according to response surface methodology (RSM) results. RSM was more convenient to figure out the optimized preparation condition of MBC-MFC theoretically for achieving a maximum removal efficiency of Cr(VI) and total chromium (T_{Cr}), compared to labor-intensive orthogonal experiments. The RSM results showed that Fe/Mn concentration (C_{Fe}; C_{Mn}), MBC activation temperature after soaking in KOH solution (T), and pH during precipitation of Fe-Mn oxide were three main factors to significantly affect the efficiency of MBC-MFC ($p < 0.05$) in Cr(VI) and T_{Cr} removal. With the selected condition (C_{Fe} = 0.28 mol/L; C_{Mn} = 0.14 mol/L; T = 790°C; pH = 9.0), MBC-MFC was synthesized with a large surface area (318.53 m^2/g), and the point of zero charge values of MBC-MFC was 5.64. The fabricated MBC-MFC showed excellent adsorption performance of Cr(VI) and T_{Cr} in an aqueous solution. The maximum Cr(VI) and T_{Cr} removal capacity of MBC-MFC was 56.18 and 54.97 mg/g (T = 25°C, pH = 3.0, t = 48 h, and dosage = 0.10 g/50 ml), respectively, and the maximum Cr(VI) adsorption of MBC-MFC was 4.16 times that of bare MBC, suggesting the synergistic effects of Fe/Mn oxides and MB on the performance of MBC-MFC in Cr(VI) and T_{Cr} removal. The adsorption mechanism of MBC-MFC on chromium was mainly contributed by surface complexation and electrostatic attraction. Our study offers valuable outlooks to develop high-performance biochar-based sorbents for heavy metal removal and sustainable environmental remediation.

Keywords: adsorption, chromium, Fe-Mn oxide, mulberry stem biochar, response surface model

INTRODUCTION

Toxic heavy metal ions are very harmful to human health and environmental ecosystem (Wang et al., 2020; Liu et al., 2021), among which chromium-containing compounds are among the most ubiquitous contaminants (Kretschmer et al., 2019; Pei et al., 2020; Xu et al., 2021). Chromium commonly exists in the industrial waste and natural environment in the form of Cr(III) and Cr(VI) (Andrade et al., 2019; Qiu et al., 2020; Zhang et al., 2020). Cr(III) is comparatively stable in an environment with low mobility and solubility, while Cr(VI) primarily exists in the form of oxyanions such as CrO_4^{2-}, $Cr_2O_7^{2-}$, and $HCrO_4^-$, which are highly soluble and mobile (Li et al., 2020). The toxicity of Cr(VI) is much greater than that of Cr(III) and would cause carcinogenesis in living creatures. Therefore, Cr(VI) has been identified as the top priority hazardous pollutant by the United States Environmental Protection Agency (EPA) (Lv et al., 2020; Park, 2020). The Ministry of Ecology and Environment of the People's Republic of China has set the maximum concentration of Cr(VI) for the legal discharge of surface water as 50 ug/L (Lv et al., 2020).

In order to remove the chromium from industrial wastewater, various methods have been investigated (Ma and Tsai, 2017; An et al., 2018; Zhao et al., 2018; Li et al., 2019a; Breytus et al., 2019; Ye et al., 2019; Choi et al., 2020; Tang et al., 2020), such as membrane separation, electrochemistry, chemical precipitation, photocatalysis, ion exchange, constructed wetlands, and adsorption. Among these available approaches, the adsorption method is one of the most commonly used methods based on its good adsorption capacity, recyclability, low-cost, environmental-friendly materials, and operation simplicity (Qin et al., 2020). Biochar is a kind of widely used material for chromium adsorption due to its high specific surface area and hierarchical pore structures. Biochar could be easily obtained *via* thermochemical pyrolysis of various waste biomass under an oxygen-free atmosphere, such as rice straw, algae, walnut shell, energy crops, bagasse, forest residue, and even activated sludge. Thus, biochar is regarded as a well-produced material based on widespread natural material resource with high specific surface area and hierarchical pore structures, which could prevent the agglomeration of Fe-Mn binary oxide nanoparticles and provide adsorption sites. In addition, the biochar surface contains a lot of oxygen-containing functional groups, which allowed the organic pollutants and heavy metal pollutants to be adsorbed to the surface of biochar and reduced (Liang et al., 2020; Luo et al., 2020). Biochar has been demonstrated as a promising sorbent for heavy metal adsorption (Luo et al., 2020). Guangxi Zhuang Autonomous Region is one of the provinces in China with the largest number of mulberry trees used for silkworm cultivation (Liang et al., 2020). In China, about six million tons of mulberry stem is harvested each year and conventionally used for burning, which not only wastes resources but also causes environmental pollution (Liao et al., 2018).

Iron and manganese oxides have been demonstrated to have a high adsorption affinity towards heavy metals. Besides (Aryal et al., 2011; Granados-Correa and Bulbulian, 2012), Fe-Mn mixed metal oxide nanocomposites also showed good regeneration and stability activity for Cr(VI) removal (Wang and Fu, 2013). The granular Fe-Mn binary oxide (GFMO) was prepared and the adsorption capacity of GFMO for Cr(VI) was 16.79 mg/g (Du et al., 2019). Fe-Mn bimetal oxide (IMBO) nanospheres were synthesized by template-free method and the adsorption capacity of IMBO towards Cr(VI) was 105.96 mg/g (Wen et al., 2017). Iron and manganese oxides are easy to aggregate, which would have a significant influence on their adsorption performance. Thus, they are normally loaded on biochar to inhibit their aggregation.

HA/Fe-Mn oxides-loaded biochar (HFMB) was synthesized and used to adsorb cadmium (Cd) and arsenic (As) that the maximum adsorption capacity of HFMB was 67.11 mg/g for Cd(II) and 35.59 mg/g for As(V), which is much higher than pristine biochar (11.06 mg/g and 0 mg/g for Cd(II) and As(V), respectively) (Guo et al., 2019). Liang et al. (2021) used Mn-incorporated ferrihydrite to adsorb Cr(VI) and the maximum adsorption capacity was 48.5 mg/g, which was 30% higher than pure ferrihydrite. Luo et al. (2013) also used manganese dioxide/iron oxides combined with acid oxidized multiwalled carbon to adsorb Cr(VI) and showed excellent adsorption performance for Cr(VI). Sand media simultaneously coated with iron and manganese were applied to treat synthetic wastewater contaminated with both Cr(VI) and As(V) (Chang et al., 2012). Our group (Liang et al., 2020) discovered that Fe-Mn binary oxide/mulberry stem biochar could synergistically improve the sorption of Cr(VI). In summary, the composite adsorbent consisting of manganese/iron oxides and scaffold structure with high specific surface area is beneficial to its adsorbing performance of heavy metals, and biochar has been demonstrated as a typical scaffold to load both manganese oxides and iron oxides for heavy metal adsorption. "Green" iron oxide combined with mulberry acted as a sorbent to the removal of Cr(VI) from aqueous solutions (Poguberovi´ et al., 2016). It has shown great potential to remove Cr(VI) by using the biochar and Fe-Mn binary oxide composite.

Response surface methodology (RSM) is a collection of mathematical and statistical techniques based on the fit of a polynomial equation to the experimental data, which is a useful tool to study the interactions of two or more parameters. The Plackett–Burman (RSM-PB) and the Box–Behnken (RSM-BBD) are two designs in RSM (Hanrahan and Lu, 2006), which have been used for designing and optimizing the environmental experiments. RSM-PB was designed as a two-level experimental design that requires fewer runs than a comparable fractional design and can be used to identify the more important independent variables from a long list of candidate factors and select them to realize a complete factorial design (He and Tan, 2006). RSM-BBD is a second-order multivariate technique based on three-level incomplete factorial designs that received a wide application for assessment of critical experimental conditions, that is, the maximum or minimum of response function (MourabetRhilassi et al., 2012). However, to the best of our knowledge, there are limited studies on the application of RSM in optimizing the oxidation of iron and manganese on mulberry stem biochar (MBC) for Cr(VI) removal.

In this study, the optimized preparation condition of MBC-MFC to maximize its removal rate of Cr(VI) and T_{Cr} was figured out based on RSM theoretically. Accordingly, MBC-MFC was fabricated based on the optimized condition, its performance in T_{Cr} and Cr(VI) removal was studied, and the corresponding removal mechanisms were investigated.

MATERIALS AND METHODS

Materials

All chemical reagents (viz., $KMnO_4$, $Fe(NO_3)_3{\bullet}9H_2O$, KOH, NH_4HCO_3, $K_2Cr_2O_7$, H_3PO_4, H_2SO_4, HCl, C_2H_5OH, etc.) used in this study were of analytical grade and purchased from Shanghai Guoyao Group Chemical Reagent Co. Ltd., China. Stock solution [1,000 mg/L Cr(VI)] was prepared with $K_2Cr_2O_7$ and ultrapure water and was used to prepare diluted chromium-containing solutions for adsorption experiments. 1,000 mg/L of Cr(VI) standard solution was purchased from the National Nonferrous Metals and Electronic Materials Analysis and Testing Center, China, and stored at 4°C. Ultrapure water was used to prepare all solutions.

Preparation of Mulberry Stem Biochar Composite and Mulberry Stem Biochar/Mn-Fe Binary Oxide Composite

The preparation methods of MBC and MBC-MFC were based on Chinese invention patents (Liang et al., 2019).

Preparation of MBC: the peeled mulberry was crushed into particles of less than 2 mm and finally dried in an oven (80°C) until it reached the constant weight. The dry mulberry was pyrolyzed at 450–650°C in a muffle furnace at the heating rate of 5°C/min until it reached a set temperature and maintained specified temperature for 3–6 h. The final products were denoted as MBC, which was stored in airtight glass bottles.

Preparation of MBC-MFC: some MBC was added to a conical flask containing 100 ml of 9.0–15.0 mol/L NaOH solution and stirred for 12–36 h and then filtered and dried; the dried MBC was activated at 700–900°C for 1 h. After activation, MBC was washed with ultrapure water 3–5 times and then filtered, and the filter cake was placed in a porcelain dish and dried at 110°C for 6 h to obtain the MBC intermediate. 3–6 g MBC intermediate was added to a 500 ml conical flask and oscillated with an ultrasonic oscillator at a frequency of 25–45 kHz for 30 min; then, the conical flask was put into a magnetic constant temperature water bath at 25°C. Under the magnetic stirring condition, 50 ml of 0.05–0.15 mol/L $KMnO_4$ solution and 50 ml of 1.0–1.5 mol/L NH_4HCO_3 solution were added to the conical flask and stirred for 15 min; immediately after, 50 ml of 0.1–0.3 mol/L $Fe(NO_3)_3$ solution was added to the conical flask, and then the pH of mixture suspension was adjusted to 7.5–10.5 with 1.0 mol/L NaOH solution. Next, the conical flask was put into a water bath at 95°C reacted for 4–8 h, after being cooled to room temperature, filtered, and washed three times with ultrapure water and one time with absolute ethanol. The filter cake was placed in a porcelain dish and dried at 85°C for constant weight to get the MBC-MFC; then, the MBC-MFC was ground and sifted by a 200-mesh sieve.

Optimization of Preparation Conditions Through RSM

RSM is employed to optimize the preparation conditions in this work to study the effects of pH, temperature, concentration, and time on T_{Cr} and Cr(VI) removal efficiency of MBC-MFC. RSM-PB was used to figure out the main factors from various factors that affect the removal rate of sorbent from lots of variables (He and Tan, 2006), and RSM-BBD was employed to optimize those main factors to obtain the best conditions for fabricating MBC-MFC with excellent performance to adsorb T_{Cr} and Cr(VI) (Liang et al., 2019).

RSM-PB in RSM

The thermochemical pyrolysis temperature (Wang and Wang, 2019), residency time (Rogovska et al., 2012), heating rate (Rogovska et al., 2012), and heating method (Liang et al., 2017) of biochar have a great influence on the number of functional groups on biochar. Moreover, nanocomposite sorbents with nanosized metal oxyhydrates are attached to carbonaceous surfaces within biochar and increase the sorption of contaminants (Ahmed et al., 2016). In this paper, eight parameters for MBC-MFC preparation (**Supplementary Table 1**) have been evaluated for their effects on the removal rate of T_{Cr} and Cr(VI). All preparation factors in **Supplementary Table 1** were set on the basis of previous single factor experiment to make the obtained results under critical conditions, such as the chosen variables ranges, batch experiment conditions, and the applied concentrations.

RSM-BBD in RSM

Based on the results of RSM-PB, we selected three main factors for MBC-MFC preparation and their effects on the removal rate of T_{Cr} and Cr(VI), which was described as **Eq.1** (Grady and Kenneth, 2006). The three selected factors were defined as X_1, X_2, and X_3, respectively. They were coded at three levels, −1 (minimum), 0 (central), and +1 (maximum), covering the whole range of interest (**Supplementary Table 2**). The data in **Supplementary Table 2** represent the factors and their level ranges in RSM-BBD.

$$Y = \beta_0 + \beta_1 X_1 + \beta_2 X_2 + \beta_3 X_3 + \beta_{12} X_1 X_2 + \beta_{13} X_1 X_3 + \beta_{23} X_2 X_3 + \beta_{11} X_1^2 + \beta_{22} X_2^2 + \beta_{33} X_3^2, \quad (1)$$

where Y is the estimated response (i.e., the removal rate of Cr(VI) and T_{Cr}); β_0 is the intercept; β_1, β_2, and β_3 are the linear coefficients; β_{12}, β_{13}, and β_{23} are the squared coefficients; β_{11}, β_{22}, and β_{33} are the quadratic coefficients.

Adsorbent Characterization

The morphological structures of MBC and MBC-MFC (under the optimal conditions' preparation) were analyzed by scanning electron microscopy combined with energy dispersive

spectrum analysis (SEM-EDS) (Hitachi, JSM-7900F, Japan). X-ray diffractometer (XRD) (PANalytical, X'Pert PROX, Netherlands) and X-ray photoelectron spectroscopy (XPS) (Thermo Fisher Scientific, ESCALAB 250Xi, United States) analyses were used to identify the adsorbent constituents. A Fourier transform infrared spectrometer (FT-IR, PerkinElmer, Llantrisant, United Kingdom) was employed to collect spectra in the 400 and 4,000 cm^{-1} regions to identify the surface functional groups. The surface zeta potentials of MBC-MFC and MBC were measured by a Nano-ZS90 apparatus (Malvern Panalytical, Nano-ZS90, United Kingdom). Specific surface area, pore size distribution, and pore volume were performed by a JW-BK200C apparatus (BET-N_2) (Beijing Jingwei Gaobo, JW-BK200C, Beijing, China).

Batch Adsorption Experiments

The batch adsorption experiments were investigated by adding 0.10 g MBC-MFC to a series of 100 ml polyethylene plastic centrifuge tubes containing 50 ml of 45 mg/L Cr(VI) solutions, which were adjusted to a certain pH with 0.1 mol/L NaOH or 1.0 mol/L HCl. The centrifuge tubes were sealed by paraffin. Then they were shaken (at 180 rpm) for 48 h at 25°C. After being shaken for 48 h, samples were taken out and filtered through 0.22 um nylon membrane into a vial. The remaining Cr(VI) or T_{Cr} concentrations in the diluted were measured by ICP-OES. Unless otherwise noted, initial pH, contact time, the temperature, initial Cr(VI) concentration, and adsorbents dosage of all batch experiments were 3.0 ± 0.1, 48 h, 25°C, 60 mg/L, and 0.10 g/50 ml, respectively. The batch adsorption experiments with different pH values (2.0–11.0), different contact time (0.25, 0.5, 1, 2, 3, 4, 6, 8, 10, 12, 18, 24, 30, 36, and 48 h), different temperature (25, 35, and 45°C), and different MBC-MFC dosage (0.02, 0.05, 0.10, 0.15, 0.2, 0.25, 0.3, 0.35, 0.40 g/50 ml) were carried out. The batch adsorption experiments for optimization of preparation conditions through RSM were carried out too, in which the initial Cr(VI) concentration was 45 mg/L.

Desorption and Regeneration of Adsorbent

Desorption Studies

After Cr(VI) adsorption reached equilibrium, 0.1 g of MBC-MFC was added to a 100 ml plastic centrifuge tube; then, 50 ml of the regeneration solution of HCl or NaOH solution (0.1, 0.3, or 0.5 mol/L) was added and shaken for 48 h at 25°C. After 4 h, the concentrations of desorbed Cr(VI) and T_{Cr} in the solution were measured.

Regeneration and Reuse of Adsorbent

In order to test the reusability of MBC-MFC, three consecutive adsorption-regeneration cycles were performed in triplicate. During the adsorption process, 0.10 g of MBC-MFC was added to 50 ml Cr(VI) solution and shaken for 48 h. The regeneration method was carried out as follows: the used adsorbent was collected and gently washed with deionized water, dispersed into 50 ml of a regenerative solution (0.1, 0.3, and 0.5 mol/L HCl or NaOH), and shaken for 48 h. The concentration of desorbed Cr(VI) and T_{Cr} in the solution was also measured. Lastly, the adsorbent after desorption was collected and washed with deionized water about pH = 7.0 for the next cycle.

RESULTS AND DISCUSSION

Optimization of Mulberry Stem Biochar/Mn-Fe Binary Oxide Composite by RSM-PB and RSM-BBD

Optimization by RSM-PB

The experimental scheme in **Supplementary Table 3** was obtained through the RSM-PB, and twelve kinds of MBC-MFC were prepared under different conditions. The removal rate of T_{Cr} and Cr(VI) by the MBC-MFC was used as an index to evaluate its adsorption performance. The mean values of T_{Cr} and Cr(VI) removal rate were shown in **Supplementary Table 3**, which were analyzed by Minitab software and a response model was established accordingly. The results of the analysis of variance were shown in **Supplementary Table 4**. In Cr(VI) response model, the coefficient of determination (R^2) value was 0.9956 and an adjusted $(R^2)_{Adj}$ value was 0.9839, indicating a high correlation between the actual values and the predicted values (Intani et al., 2018; Abd Manan et al., 2019). A lower *p*-value suggested that the corresponding influencing factor had a more significant effect on the adsorption performance of MBC-MFC. The order of preparation conditions factors on Cr(VI) was F > E > H > C > D > B > G > A, where F, E, H, and C were the most significant effect factors ($p < 0.01$), demonstrating that the regression equation provided strong applicability.

In the T_{Cr} response model, the R^2 value was 0.9710 and the adjusted R^2_{Adj} value was 0.8938, suggesting a high correlation between the actual results and the predicted values (Abdulhameed et al., 2019). The order of the influence of various factors on T_{Cr} was F > E > H > G > C > A > B > D, where F, E, and H were the most significant influence factors ($p < 0.05$), indicating that the regression equation provided strong applicability.

The main factors ($p < 0.05$) of standardized Pareto graphs were shown in **Supplementary Figure 1** (Vasiee et al., 2016; Ma et al., 2016). Factors such as F, E, H, and C were significant factors affecting the removal rate of Cr(VI), as shown in **Supplementary Figure 1A**, while F, E, and H were significant factors affecting the removal rate of T_{Cr}, shown in **Supplementary Figure 1B**. Thus, we propose that F, E, and H are the most significant factors to affect the removal rate of T_{Cr} and Cr(VI). Therefore, F, E, and H factors were used as the main factors for RSM-BBD (Vasiee et al., 2016). Due to the fact that the other influence factors were not significant, the optimal preparation conditions of the previous single factor experiment were adopted. Thus, A, B, C, D, and G were set at 5.70 mol/L, 450°C, and 3, 12, and 4 h, respectively.

Optimization by RSM-BBD

According to the results of **Supplementary Figure 1**, the factors in RSM-BBD of X_1', X_2', and X_3' were E, F, and H, respectively. The experimental scheme in **Supplementary Table 5** was obtained through the RSM-BBD, and 17 kinds of MBC-MFC were prepared under preparation conditions described in **Supplementary Table 5**. Except that the Cr(VI) concentration was 60 mg/L, other experimental conditions and methods were the same as RSM-PB. The observed and predicted mean removal rates of T_{Cr} and Cr(VI) are shown in **Supplementary Table 5**.

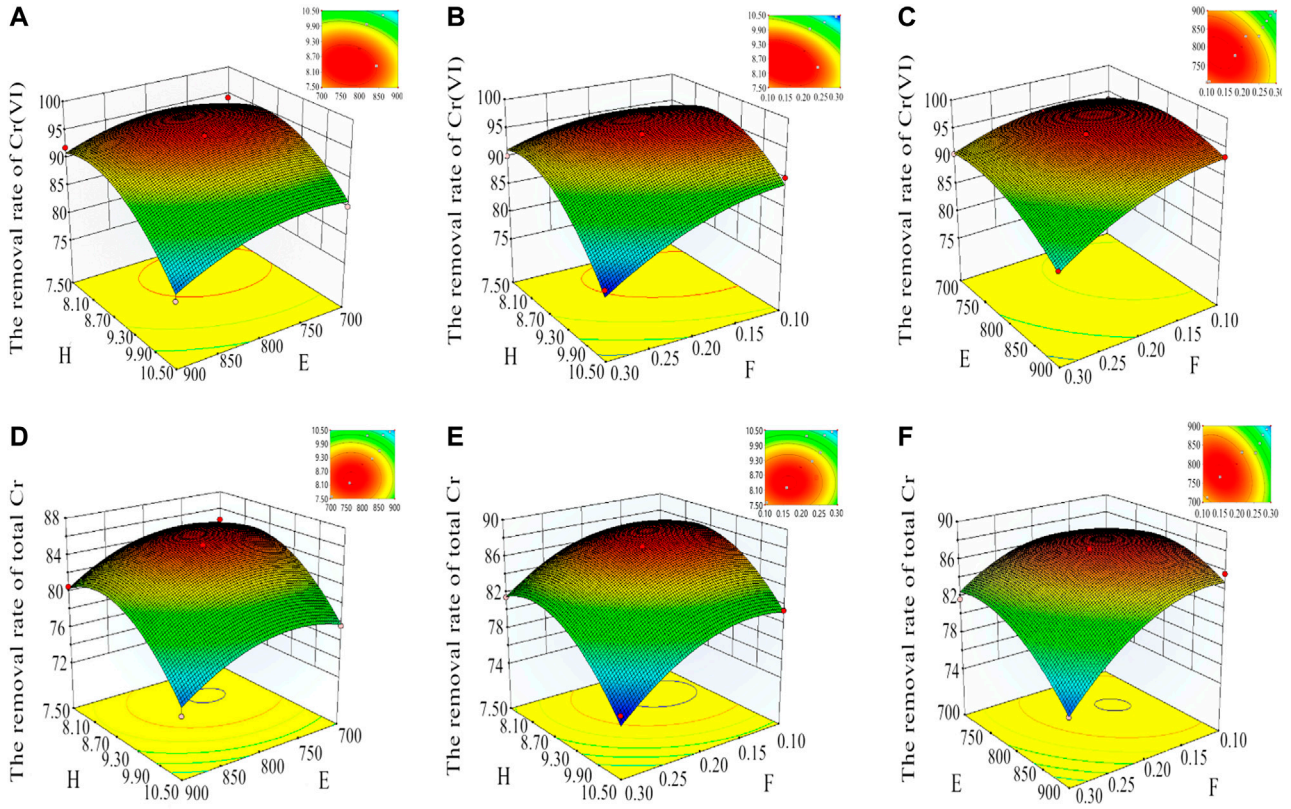

FIGURE 1 | The response surface plots and contour plots that mutually influence factors for the removal rate of T_{Cr} and Cr(VI). **(A–C)** are for Cr(VI), and **(D–F)** are for T_{Cr} (A, B, C, D, E, F, G, and H were set at the concentration of KOH (mol/L), MBC carbonization temperature (ºC), MBC carbonization time (h), MBC soaking time with KOH (h), MBC activation temperature after soaking in KOH solution (ºC), Fe/Mn concentration (C_{Fe}, C_{Mn}) (mol/L), reaction time (h), and the pH during precipitation of Fe-Mn oxide, respectively).

In the Cr(VI) and T_{Cr} response model, Design-Expert 8.0.6 software was employed to perform quadratic regression fitting the data in **Supplementary Table 5**, and the result of ANOVA for response function was presented in **Supplementary Table 6**. From the ANOVA table (**Supplementary Table 6**), it is evident that all the terms are significant because of their low *p*-values and high F-values. The *p*-values are <0.0001 and the F-values are 30.14 and 28.58 for Cr(VI) and T_{Cr}, respectively, indicating that the model terms are significantly different. The F-value of lack-of-fit (Cr(VI) of 4.61; T_{Cr} of 2.59) revealed that the lack-of-fit was not significant (*p*-value = 0.0871) (Kuan et al., 2019). The Cr(VI) and T_{Cr} removal efficiency by MBC-MFC can be predicted using the following reduced quadratic model:

$$\begin{aligned} Y_{Cr(VI)}(\%) = &-327.37 + 0.51\,E + 342.74\,F + 46.66\,H \\ &- 0.18\,EF - 15.50\,FH - 7.48\,E - 003\,EH \\ &- 232.25\,F^2 - 2.67\,E - 004\,E^2 - 2.25\,H^2, \end{aligned} \quad (2)$$

$$\begin{aligned} Y_{TCr}(\%) = &-212.10 + 240.66\,F + 0.41\,E + 29.03\,H \\ &- 0.16\,EF - 4.15\,FH - 4.67\,E - 004\,EH \\ &- 265.95\,F^2 - 2.44\,E - 004\,E^2 - 1.66\,H^2, \end{aligned} \quad (3)$$

One independent variable factor of F, E, and H was kept at a fixed level (coded value was 0) to analyze the influence of interaction between other variables on the adsorption capacity of Cr(VI) and T_{Cr} on MBC-MFC. Accordingly, a 3D (three-dimensional response surfaces) surface map and 2D (plotting two-dimensional contour lines) profile could be obtained (Jang and Lee, 2018), as shown in **Figures 1A–C** and **Figures 1D–F**. **Figure 1A** showed the interaction between E (700–840˚C) and H (pH = 7.6–9.2), while F was kept at a fixed level. **Figure 1B** showed the interaction between F (C_{Fe} = 0.10–0.24 mol/L; C_{Mn} = 0.05–0.12 mol/L) and H (pH = 7.6–9.4), while E was kept at a fixed level. **Figure 1C** showed the interaction between E (740–820˚C) and F (C_{Fe} = 0.10–0.18 mol/L; C_{Mn} = 0.05–0.09 mol/L).

Using the same analysis method as **Figures 1D–F**, the condition of E was selected at 700–850˚C; F was C_{Fe} = 0.10–0.24 mol/L, C_{Mn} = 0.05–0.12 mol/L, and H was 7.5–9.4. According to analysis results of RSM, the best optimized synthesis conditions of MBC-MFC were determined: E, F, and H were set at 790˚C, 0.14 mol/L, and 9.0, respectively. Through **Figure 1**, we can intuitively see that the preparation conditions have great effects on the adsorption capacity of Cr(VI) and T_{Cr} on MBC-MFC.

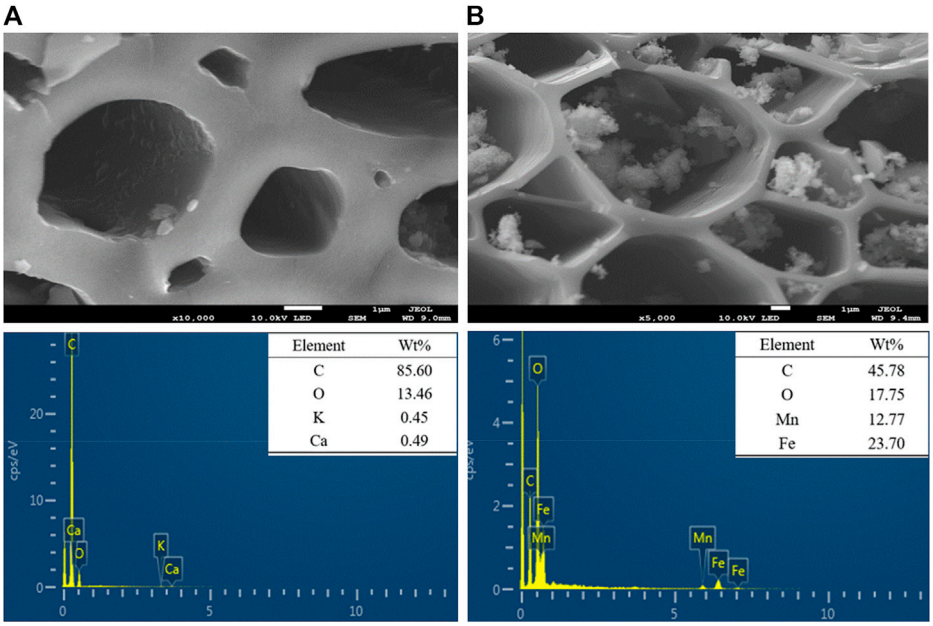

FIGURE 2 | Surface composition of MBC and MBC-MFC by SEM-EDS analysis. **(A)** MBC; **(B)** MBC-MFC.

Validation of the Model

The optimal values of the selected variables were got by solving the equation (**Eqs. 2**, **3**) using Design-Expert 8.0.6 software: A, B, C, D, E, F, G, and H were set at 5.70 mol/L and 9 mol/L, 450°C, 3 and 12 h, 790°C, C_{Fe} = 0.28 mol/L, C_{Mn} = 0.14 mol/L, 4 h, and 9.0, respectively. The theoretical removal rates predicted under the above conditions were 95.13 and 87.2% to Cr(VI) and T_{Cr}, respectively. However, the experiment mean removal rates were 96.47 and 88.63% to Cr(VI) and T_{Cr}, respectively. The relative deviation between the predicted value and the experimental value was 1.40 and 1.64%, respectively, proving the validity of our model.

Characterization of Mulberry Stem Biochar Composite and Mulberry Stem Biochar/ Mn-Fe Binary Oxide Composite

According to the results measured by BET-N_2, the surface area of MBC and MBC-MFC was 179.29 and 318.53 m^2/g, respectively, and the total pore volume of MBC-MFC (0.337 cm^3/g) was 2.6 times that of MBC (0.132 cm^3/g). Increasing surface area and total volume are considered as one of the favorable conditions for improving the adsorption capacity of MBC-MFC.

The SEM-EDS images (**Figure 2**) revealed that there were lots of pores with different sizes on the surfaces of MBC and MBC-MFC. Some Fe-Mn oxides were loaded on the surface of MBC-MFC with the porous structure not being disrupted (**Figure 2B**), which will be of great benefit to Cr(VI) and T_{Cr} adsorption. The chemical composition of MBC-MFC showed that the elemental molar ratio of Fe to Mn was close to 2:1, the same as that of the preparation precursor. The EDS analysis showed that the content of O (17.75%) in MBC-MFC was significantly higher than that of MBC (13.46%), suggesting that MBC-MFC owned more adsorption sites for heavy metal complex adsorption (Liu et al., 2020a).

XRD patterns of MBC and MBC-MFC are illustrated in **Figure 3A**. As shown, the peaks of the MBC-MFC at 24.13°, 33.12°, 35.60°, 40.82°, 49.41°, 54.00°, and 62.38° were corresponding to lattice planes of (012), (104), (110), (113), (024), (116), and (214) of Fe_2O_3 (JCPDS NO: 089–0,597), and the peaks at 20.35°, 30.92°, 33.53°, 41.75°, and 45.01° were corresponding to lattice planes of (021), (110), (023), (131), and (132) of Mn_3O_4 (JCPDS NO: 065–1,123), confirming the presence of crystalline Fe_2O_3 and Mn_3O_4 within MBC-MFC. In addition, the broad peak around at 2θ = 26.60° was corresponding to amorphous carbon (Liu et al., 2020b). The XPS spectra of MBC and MBC-MFC are shown in **Figure 3B**. The distinct peaks of Fe and Mn could only be observed on MBC-MFC, which confirmed the successful fabrication of Fe_2O_3 and Mn_3O_4 on MBC.

The FT-IR spectra of MBC and MBC-MFC were as shown in **Figure 3C**. The peak appearing at 3,391–3,422 cm^{-1} and 1,569–1,639 cm^{-1} was related to the stretching of -OH groups and C=O, respectively, indicating that both MBC and MBC-MFC contained C=O and -OH groups. The bending vibration at about 1,383 cm^{-1} was mainly contributed by the stretching vibration of Fe-O-Mn, and the bands at 1,118 cm^{-1} were associated with the bending vibration of hydroxyl groups of metal oxides (M-OH) (Du et al., 2017). MBC-MFC showed additional broadband at 595 cm^{-1}, relating to the stretching vibration of Fe-O-Fe (Luo et al., 2013). Therefore, the SEM-EDS, FT-IR, and XRD spectra confirmed that iron oxide and manganese oxide were successfully coated on the surface of MBC-MFC.

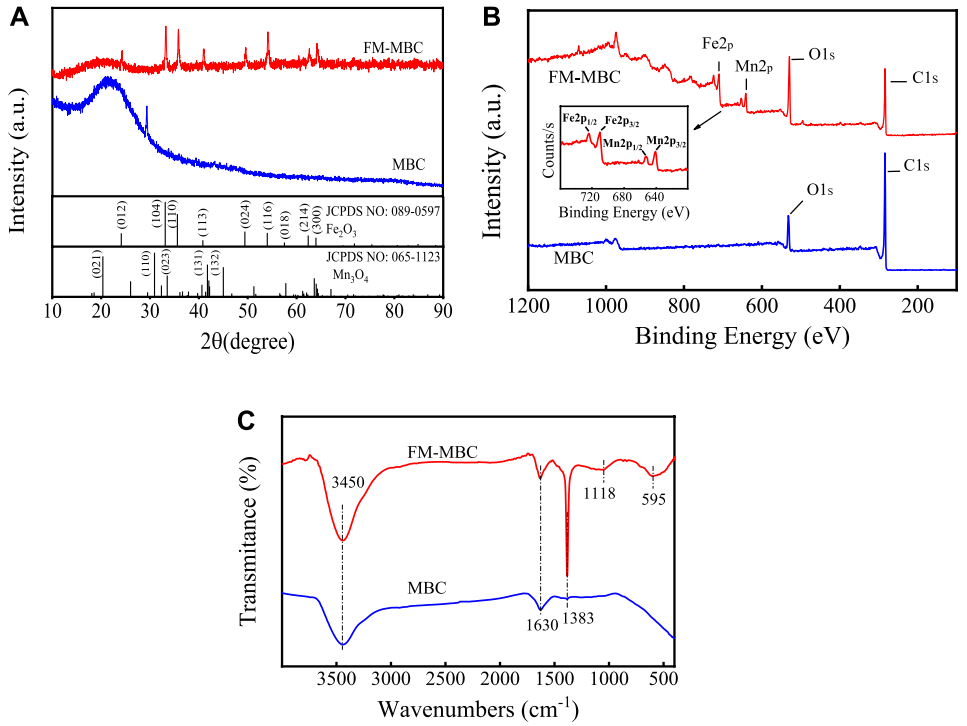

FIGURE 3 | Spectra of MBC and MBC-MFC. **(A)** XRD, **(B)** XPS, and **(C)** FT-IR.

Cr(VI) Removal by Mulberry Stem Biochar Composite and Mulberry Stem Biochar/Mn-Fe Binary Oxide Composite

The pH effects on the surface electronegativity and corresponding Cr(VI) adsorption of adsorbent were studied. When the pH ≤ 2.0, Cr contaminant mainly existed in the form of H_2CrO_4. With the increase of pH (2.0 ≤ pH ≤ 6.4), it mainly existed in the form of $HCrO_4^-$ and $Cr_2O_7^{2-}$. By further increase in the pH (pH ≥ 6.4), it mainly existed in the form of CrO_4^{2-} Liu et al., 2021. As illustrated in **Supplementary Figure 2**, the pH_{ZPC} of MBC-MFC was 5.64. When pH < pH_{ZPC} (5.64), the functional groups of absorbent were protonated and positively charged, promoting the adsorption of chromium ions onto the MBC-MFC surface. When pH > pH_{ZPC} (5.64), the surface of the adsorbent was negatively charged, which weakens the attraction for Cr(VI). In addition, a higher pH would tend to generate more OH^-, which would occupy some of the adsorption sites, thereby reducing the amount of Cr(VI) adsorption on MBC-MFC (Chen et al., 2018).

The effects of pH on the adsorption of Cr(VI) by MBC-MFC are shown in **Figure 4A**. In **Figure 4A**, when the initial Cr(VI) concentration was set at 30 and 60 mg/L, the adsorption capacity of Cr(VI) increased slowly as the pH raised from 2.0 to 3.0. The uptake of cationic metal ions by biochar at pH 2.0 was lower than that at pH 3.0 (Senthilkumar et al., 2019). Further enhancement of equilibrium pH negatively influenced the adsorption capacity of MBC-MFC (3.0 < pH < 9.0). It shows that ion exchange and electronic interaction may be involved in the adsorption mechanism of Cr(VI) (Choudhary and Paul, 2018). The optimal pH value for MBC-MFC to adsorb Cr(VI) varies with the initial Cr(VI) concentration. When the initial Cr(VI) concentration was 30 mg/L, the best initial pH range was 2.0–5.0. When the initial Cr(VI) concentration was 60 mg/L, the best initial pH range was 2.0–3.0. When the pH value was in the range of 8–11, the adsorption capacity of Cr(VI) was relatively low and basically remains unchanged, which was similar to the results of Chen et al. (2018). The pH of the subsequent experiments was 3.0.

The effects of contact time on adsorption are shown in **Figure 4B**. It can be seen from **Figure 4B** that, with the increase of the adsorption time, the adsorption capacity of Cr(VI) increases, but with the extension of time, the adsorption capacity gradually reaches equilibrium. In the initial stage of adsorption, due to the large number of pores on the surface of MBC-MFC, it can provide more binding sites, and it was easy to adhere to the surface of MBC-MFC after adsorption. As the contact time increases, the number of adsorption binding sites decreases, making it difficult for the adsorption reaction to continue, thus reaching adsorption equilibrium (Zhang et al., 2018). When the initial concentrations were 30, 45, and 60 mg/L, the adsorption equilibrium was reached after 420, 960, and 1,440 min, and the removal rates were 99.2, 99.7, and 99.3%, respectively. With the increase of Cr(VI) concentration, the electrostatic

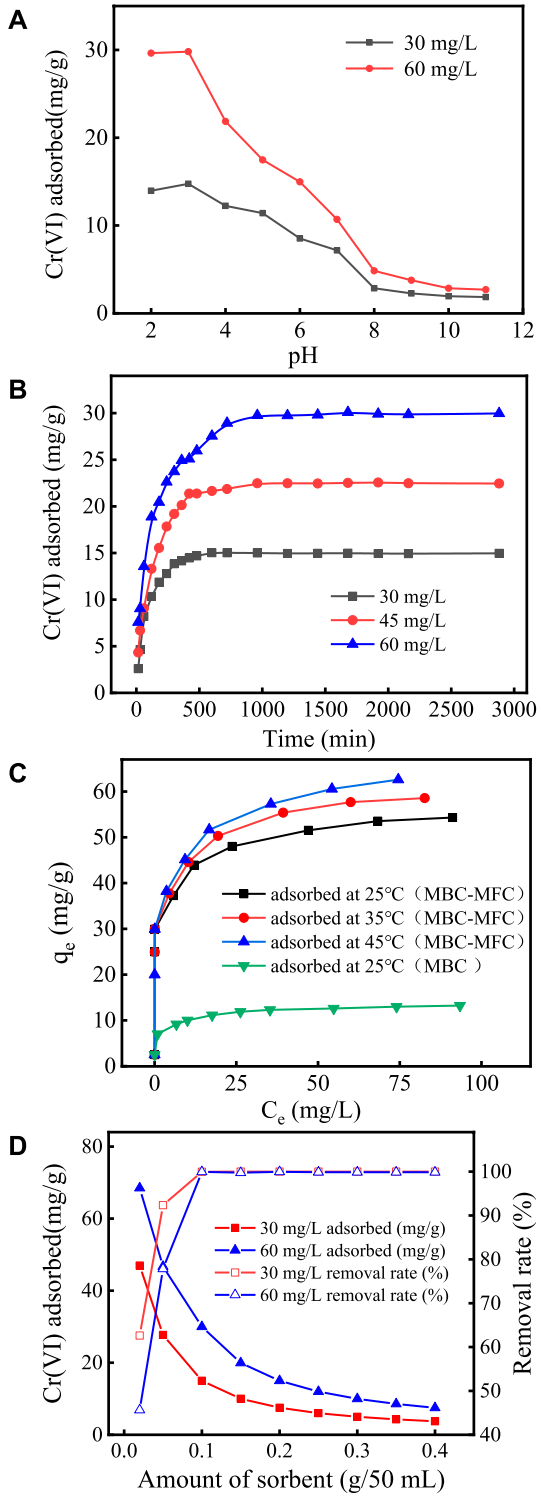

FIGURE 4 | Cr(VI) and T_{Cr} removal of MBC-MFC. **(A)** Effect of pH. **(B)** Effect of contact time at pH 3.0. **(C)** Effect of temperatures at pH 3.0. **(D)** Effect of dosage at pH 3.0.

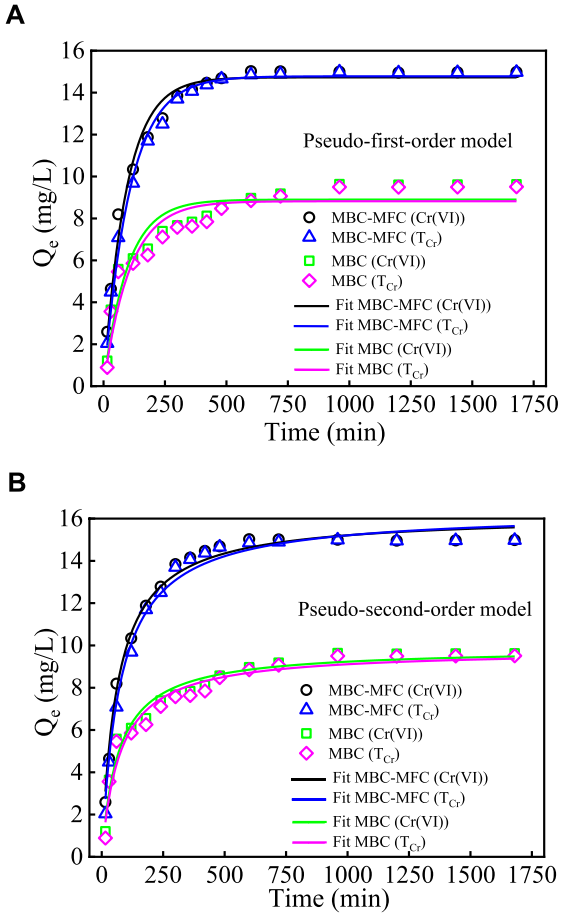

FIGURE 5 | The Cr(VI) and T_{Cr} removal kinetics fitted with pseudo-first-order model and pseudo-second-order model (T = 25°C, pH = 3.0, and C_0 [Cr(VI)] = 30 mg/L). **(A)** pseudo-first-order model. **(B)** pseudo-second-order model.

repulsion between ions increases, so the adsorption equilibrium time was prolonged (Mondal et al., 2007; Park, 2020). After reaching the adsorption equilibrium, the equilibrium adsorption capacity of initial concentrations of 30, 45, and 60 mg/L was about 14.97, 22.46, and 29.97 mg/g, respectively.

The effects of temperature on adsorption are shown in **Figure 4C**. As shown in **Figure 4C**, the maximum adsorption capacity of MBC and MBC-MFC for Cr(VI) was 12.84 mg/g and 54.31 mg/g at 25°C, respectively. Compared with MBC, the adsorption capacity of MBC-MFC on Cr(VI) has been greatly improved, which was 4.16 times that before modification. At 25, 35, and 45°C, the equilibrium adsorption capacity of MBC-MFC for Cr(VI) was about 54.31, 58.57, and 62.60 mg/g, respectively.

The effects of MBC-MFC dosage on chromium adsorption are shown in **Figure 4D**. In **Figure 4D**, when the initial concentration of Cr(VI) was set at 30 mg/L, with the increase of the dosage from 0.02 g/50 ml to 0.40 g/50 ml, the adsorption capacity decreased from

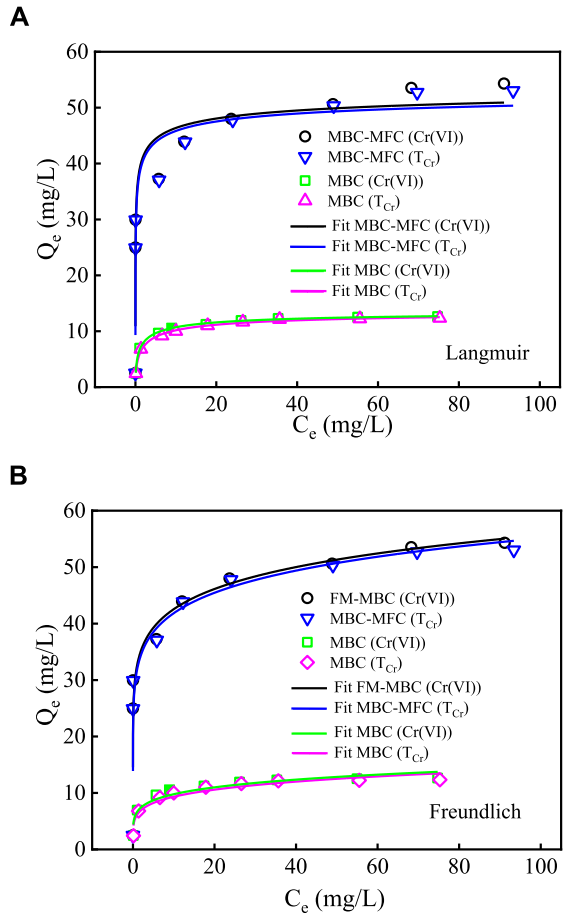

FIGURE 6 | The Cr(VI) and T_{Cr} removal isotherm fitted with Langmuir and Freundlich (T = 25°C; pH = 3.0). **(A)** Langmuir. **(B)** Freundlich.

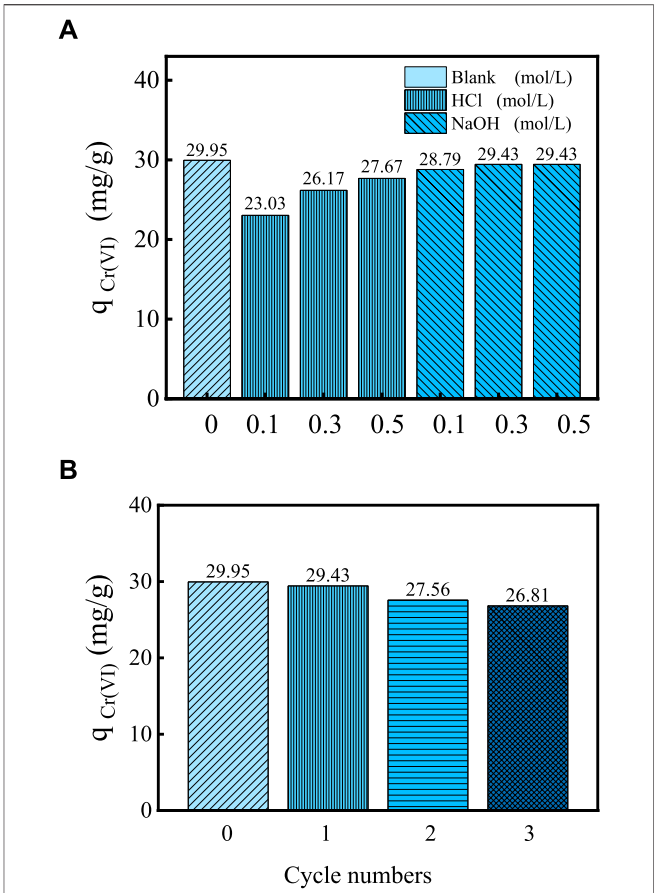

FIGURE 7 | Desorption and regeneration of Cr(VI) sorption onto MBC-MFC. (MBC-MFC dosage = 0.10 g/50 mL, C0 (Cr(VI)) = 60 mg/L, T = 25°C, pH = 3.0). **(A)** Desorption Studies. **(B)** Regeneration and Reuse of Adsorbent.

46.97 to 3.75 mg/g, and when the initial concentration of Cr(VI) was set at 60 mg/L, the adsorption capacity decreased from 68.50 to 7.45 mg/g. The adsorption capacity of Cr(VI) decreased with the increase of the dosage, while the removal rate of Cr(VI) increases with the increase of the dosage. When the initial concentration of Cr(VI) was set at 60 mg/L, the removal rate increased from 45.66 to 99.98%. When the dosage was greater than 0.10 g/50 ml, the removal rate did not increase. The reason may be that, with the increase of the dosage, the total reaction sites on the sorbent surface were increased (Tang et al., 2021). Therefore, the effective dosage for Cr(VI) was selected at 0.10 g/50 ml for the latter experiments.

In this study, we employed a pseudo-first-order kinetic model and pseudo-second-order kinetic model to study the Cr(VI) adsorption kinetic onto MBC-MFC and MBC. The fitting plots are shown in **Figures 5A,B**, respectively, and the kinetic parameters are summarized in **Supplementary Table 7**. The pseudo-second-order kinetic model better fitted the experimental data of the Cr(VI) and T_{Cr} removal by the MBC-MFC and MBC (R^2 = 0.957–0.989) and the Cr(VI) equilibrium adsorption capacities (14.97, 14.96, 9.61, and 9.50 mg/g) calculated by the pseudo-second-order kinetic model was approximately equal to the Cr(VI) experimental adsorption capacities data (14.98, 14.97, 8.90, and 8.82 mg/g) (Pap et al., 2018).

Figure 6 shows the application of Langmuir and Freundlich isotherms to the Cr(VI) adsorption on MBC-MFC and MBC. **Supplementary Table 8** lists the isotherms parameters. The Langmuir model better fitted the experimental data of the MBC-MFC and MBC (R^2 = 0.909–0.998) than the Freundlich model, which may imply monolayer adsorption of Cr(VI) and T_{Cr} (Wen et al., 2018). The MBC-MFC exhibited superior T_{Cr} and Cr(VI) adsorption capacity than MBC. The maximum T_{Cr} and Cr(VI) adsorption capacities (q_m) of the MBC-MFC reached 54.97 and 56.18 mg/g, respectively. It was about 4.11 times that of MBC, which is 5.61 times that of dolomite adsorbent (Albadarin et al., 2012), 2.64 times that of *Eucalyptus globulus* bark biochar (Choudhary and Paul, 2018), 8.03 times that of biochar derived from municipal sludge (Chen et al., 2015), slightly higher than 2.64 times that of *Eucalyptus globulus* bark biochar (Zhang et al., 2018), and 2.14 times of Fe/Mn metal oxide nanocomposites (Yacou et al., 2018; **Supplementary Table 9**). The adsorption capacity of Cr(VI) was calculated based on the remaining amount of Cr(VI) in solution, while the adsorption capacity of T_{Cr} was calculated based on the remaining amount of chromium in solution. According to our result, the maximum

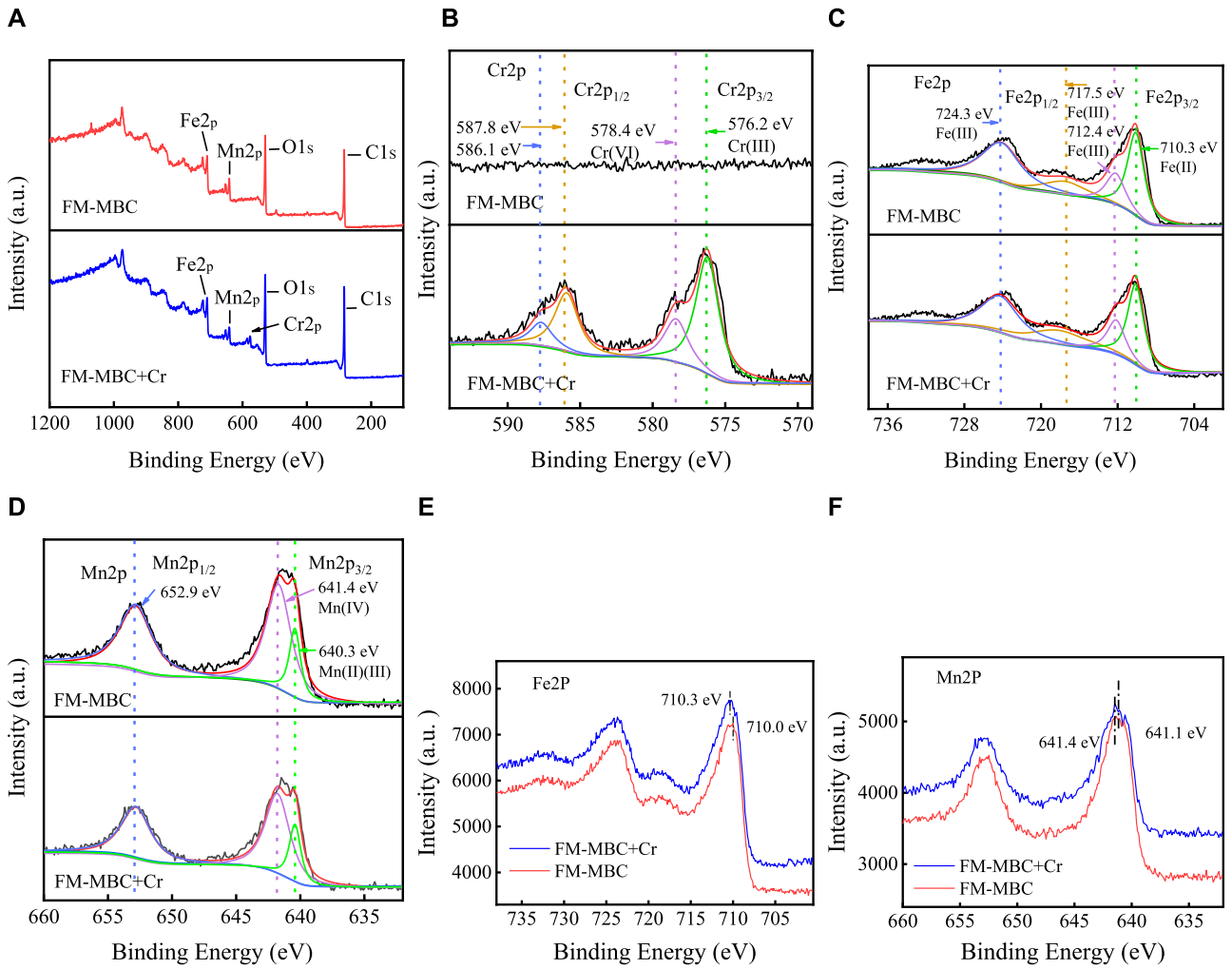

FIGURE 8 | XPS spectra for MBC-MFC and MBC-MFC + Cr. **(A)** survey; **(B)** Cr2p; **(C, E)** Fe2p; **(D, F)** Mn2p.

adsorption capacity of Cr(VI) was 2.20% higher than that of T_{Cr}, indicating the existence of a little Cr(III) in the solution. The Cr(III) in solution after adsorption was originated from the redox reaction of Cr(VI) (Lv et al., 2012).

Regeneration and Reusability Study

Strong acids and base are the most common agents used to elute heavy metals, and the choice of eluent depends on the adsorption mechanism of heavy metals and the nature of the adsorbents (Markovski et al., 2014). The results of desorption experiments are shown in **Figure 7A**. It can be seen from **Figure 7A** that 0.1, 0.3, and 0.5 mol/L HCl were used as the desorption solvent, and the adsorption capacity of Cr(VI) by the adsorbent after desorption was 23.03, 26.17, and 27.67 mg/g, respectively. However, 0.1, 0.3, and 0.5 mol/L NaOH were used as the desorption solvent, and the adsorption capacity of Cr(VI) by the adsorbent after desorption was 28.79, 29.43, and 29.43 mg/g, respectively. Therefore, NaOH solution performed a better desorption effect than HCl solution as the regeneration reagents. Considering the cost factor, a 0.3 mol/L NaOH solution was selected as the desorption solution for the desorption regeneration of MBC-MFC.

The MBC-MFC desorption and resorption experiment is shown in **Figure 7B**. It can be seen from **Figure 7B** that as the number of desorption cycles increases, the adsorption amount of Cr(VI) also decreases. It can be attributed to the following reasons: ① The specific surface area (effective adsorption point) of the adsorbent was gradually decreasing during the adsorption-desorption cycle. ② During the adsorption-desorption cycle, the functional groups on the surface of the adsorbent were gradually weakened, but there were still a certain number of functional groups that play a role in adsorption (Li et al., 2016). After three cycles of adsorption/desorption experiment, the adsorption capacity of Cr(VI) showed little effect on Cr(VI) adsorption, which was only slightly reduced from 29.95 to 26.81 mg/g.

It shows that MBC-MFC can be regenerated and reused by NaOH solution, which also fully shows that the interaction between adsorbent and adsorbate mainly depends on electrostatic adsorption, which was consistent with the aforementioned characterization analysis and kinetic experiment analysis results (Yu et al., 2020).

Mechanisms for Cr(VI) and T_{Cr} Adsorption

Figure 8A presents the survey XPS spectra of MBC-MFC before and after Cr(VI) adsorption. The element of Cr (576.2; 578.4 eV) was absent in the MBC-MFC result. However, it appeared on the XPS spectra of MBC-MFC after Cr(VI) adsorption, demonstrating the successful adsorption of Cr onto MBC-MFC. To further understand the Cr(VI) adsorption on MBC-MFC, high-resolution Cr2p spectra were measured, shown in **Figure 8B**. Obviously, no chromium peak was found on MBC-MFC before Cr(VI) adsorption. The broad peak of $Cr2p_{3/2}$ was found on the XPS result of MBC-MFC, which could be deconvoluted into peaks at binding energies of 578.4 and 576.2 eV, corresponding to the characteristic peaks of Cr(VI) and Cr(III) (Chen et al., 2017; Zhong et al., 2020). The areas of the two peaks indicate that Cr(VI) is partially reduced to Cr(III) (Wang et al., 2019). The high-resolution Cr2p spectra demonstrated the coexistence of Cr(III) and Cr(VI) on the microspheres of MBC-MFC. MBC-MFC can adsorb both Cr(III) and Cr(VI). We believe that there was a reduction of Cr(VI) to Cr(III) in the experiments.

In order to understand the adsorption mechanism of Cr(VI) on MBC-MFC, Fe2p and Mn2p peaks of MBC-MFC and after Cr(VI) adsorption were measured (**Figures 8C–F**). The observed two asymmetric peaks located at 710.3 and 724.3 eV could be ascribed to $Fe2p_{3/2}$ and $Fe2p_{1/2}$, respectively. For $Fe2p_{3/2}$, the peak at 710.3, 712.4, and 717.5 eV was attributed to Fe(II) and two forms of Fe(III), respectively (Li et al., 2019b). The binding energy of 710.0 eV ($Fe2p_{3/2}$) of Fe(II) peaks was shifted to 709.70 eV after Cr(VI) adsorption (**Figures 8C,E**), implying that the Cr(VI) adsorption occurred through bidentate ligand or monodentate interaction with iron oxide (Peng et al., 2019). The observed two asymmetric peaks located at 641.4 and 640.3 eV could be ascribed to $Mn2p_{3/2}$, respectively (**Figure 8D**). The peak at 641.4 eV was ascribed to Mn(IV), and another peak at 640.3 eV was related to Mn(II) and Mn(III) in different forms (Li et al., 2019b; Lin et al., 2017). The binding energy of 641.4 eV ($Mn2p_{3/2}$) of Mn2p peaks was reduced by 0.3 eV after Cr(VI) adsorption (**Figure 8F**), suggesting that the Cr(VI) adsorption occurred through surface complexation with Mn (Xiong et al., 2017).

In addition, chromium (CrO_4^{2-}, $Cr_2O_7^{2-}$, and $HCrO_4^-$) could be also adsorbed on the surface of MBC-MFC by electrostatic interaction or forming outer-sphere surface complexes. As illustrated in **Supplementary Figure 2**, by regulating the solution pH to be lower than the pH_{zpc} value of MBC-MFC (5.64), the zeta potential of MBC-MFC was positive and desirable for adsorption of chromium anions by electrostatic attraction.

CONCLUSION

The MBC-MFC was successfully fabricated by chemical precipitation on the carbonized mulberry stem, acting as a novel adsorbent to remove T_{Cr} and Cr(VI). RSM was employed to optimize the fabrication condition of MBC-MFC to realize the optimal removal of T_{Cr} and Cr(VI). The predicted removal rates of Cr(VI) and T_{Cr} by RSM agreed well with that of the experiment data. The MBC-MFC was demonstrated to own a high surface area (318.53 m^2/g) containing large oxygen functional groups, which provided abundant sites for T_{Cr} and Cr(VI) adsorption. In addition, the pH_{zpc} of MBC-MFC was 5.64, which makes it more suitable for adsorption of anions chromium under lower pH (such as pH = 2.0). Its maximum adsorption capacities of Cr(VI) and T_{Cr} were 56.18 and 54.97 mg/g, respectively (T = 25°C, pH = 3.0, t = 48 h, and dosage = 0.10 g/50 ml). The adsorption kinetics and isotherms demonstrated that a higher Cr(VI) removal efficiency could be achieved using our developed MBC-MFC than other biochar adsorbents due to the synergistic effects between biochar and Fe-Mn binary oxides. The adsorption mechanism of MBC-MFC on chromium was mainly contributed by electrostatic attraction and surface complexation. It should be noted that the MBC-MFC material prepared based on RSM optimization showed superior adsorption capacity of hexavalent chromium compared to MBC-MFC prepared by traditional methods. Our study offers a valuable outlook to develop high-performance biochar-based heavy metal sorbents for sustainable environmental remediation. Last but not least, taking advantage of mulberry stems as adsorbent not only saves production costs and reduces air pollution caused by burning mulberry stems but also solves the problem of resource utilization of agricultural and forestry wastes. This paper only studies the adsorption performance of MBC-MFC under indoor experiment conditions; there would be still a long way to go before its practical engineering applications due to the fact that the actual adsorption of industrial wastewater would be affected by many conditions, such as complex pollutants system and temperature variation of wastewater during different processes.

DATA AVAILABILITY STATEMENT

The raw data supporting the conclusions of this article will be made available by the authors, without undue reservation.

AUTHOR CONTRIBUTIONS

SX: adsorbent preparation, characterization, batch experiment, and writing—original draft. ML: writing—review and editing and supervision. YD: data collection, formal analysis, and investigation. DW: SEM, XPS, and XRD analyses. YZ: Plackett–Burman designs and Box–Behnken designs. LH: writing—review and editing and supervision.

FUNDING

The authors would like to express their gratitude to GXNSFP (Grant No. 2017GXNSFAA198186), the NSFC (Grants Nos. 21367010 and 51638006), and Guangxi Science and Technology Planning Project (Grant No. GuiKe-AD18126018). LH acknowledges the support from the Natural Science Foundation of Top Talent of SZTU (Grant No. 2019204).

SUPPLEMENTARY MATERIAL

The Supplementary Material for this article can be found online at: https://www.frontiersin.org/articles/10.3389/fenvc.2021.692810/full#supplementary-material

REFERENCES

Abd Manan, T. S. B., Khan, T., Sivapalan, S., Jusoh, H., Sapari, N., Sarwono, A., et al. (2019). Application of Response Surface Methodology for the Optimization of Polycyclic Aromatic Hydrocarbons Degradation from Potable Water Using Photo-Fenton Oxidation Process. *Sci. Total. Environ.* 665, 196–212. doi:10.1016/j.scitotenv.2019.02.060

Abdulhameed, A. S., Jawad, A. H., and Mohammad, A.-T. (2019). Synthesis of Chitosan-Ethylene Glycol Diglycidyl ether/TiO2 Nanoparticles for Adsorption of Reactive orange 16 Dye Using a Response Surface Methodology Approach. *Bioresour. Techn.* 293, 122071. doi:10.1016/j.biortech.2019.122071

Ahmed, M. B., Zhou, J. L., Ngo, H. H., Guo, W., and Chen, M. (2016). Progress in the Preparation and Application of Modified Biochar for Improved Contaminant Removal from Water and Wastewater. *Bioresour. Techn.* 214, 836–851. doi:10.1016/j.biortech.2016.05.057

Albadarin, A. B., Mangwandi, C., Al-Muhtaseb, A. a. H., Walker, G. M., Allen, S. J., and Ahmad, M. N. M. (2012). Kinetic and Thermodynamics of Chromium Ions Adsorption onto Low-Cost Dolomite Adsorbent. *Chem. Eng. J.* 179, 193–202. doi:10.1016/j.cej.2011.10.080

An, Q., Li, X.-Q., Nan, H.-Y., Yu, Y., and Jiang, J.-N. (2018). The Potential Adsorption Mechanism of the Biochars with Different Modification Processes to Cr(VI). *Environ. Sci. Pollut. Res.* 25, 31346–31357. doi:10.1007/s11356-018-3107-7

Andrade, J. K., Andrade, C. K., Felsner, M. L., and Anjos, V. E. (2019). Ultrasound-assisted Emulsification Microextraction Combined with Graphite Furnace Atomic Absorption Spectrometry for the Chromium Speciation in Water Samples. *Talanta* 191, 94–102. doi:10.1016/j.talanta.2018.07.067

Aryal, M., Ziagova, M., and Liakopoulou-Kyriakides, M. (2011). Comparison of Cr(VI) and As(V) Removal in Single and Binary Mixtures with Fe(III)-treated Staphylococcus Xylosus Biomass: Thermodynamic Studies. *Chem. Eng. J.* 169, 100–106. doi:10.1016/j.cej.2011.02.059

Breytus, A., Hasson, D., Semiat, R., and Shemer, H. (2019). Ion Exchange Membrane Adsorption in Donnan Dialysis. *Separat. Purif. Techn.* 226, 252–258. doi:10.1016/j.seppur.2019.05.084

Chang, Y.-Y., Lim, J.-W., and Yang, J.-K. (2012). Removal of As(V) and Cr(VI) in Aqueous Solution by Sand media Simultaneously Coated with Fe and Mn Oxides. *J. Ind. Eng. Chem.* 18, 188–192. doi:10.1016/j.jiec.2011.11.002

Chen, T., Zhou, Z., Xu, S., Wang, H., and Lu, W. (2015). Adsorption Behavior Comparison of Trivalent and Hexavalent Chromium on Biochar Derived from Municipal Sludge. *Bioresour. Techn.* 190, 388–394. doi:10.1016/j.biortech.2015.04.115

Chen, X., Zhang, W., Luo, X., Zhao, F., Li, Y., Li, R., et al. (2017). Efficient Removal and Environmentally Benign Detoxification of Cr(VI) in Aqueous Solutions by Zr(IV) Cross-Linking Chitosan Magnetic Microspheres. *Chemosphere* 185, 991–1000. doi:10.1016/j.chemosphere.2017.07.113

Chen, Y., Wang, B., Xin, J., Sun, P., and Wu, D. (2018). Adsorption Behavior and Mechanism of Cr(VI) by Modified Biochar Derived from Enteromorpha Prolifera. *Ecotoxicology Environ. Saf.* 164, 440–447. doi:10.1016/j.ecoenv.2018.08.024

Choi, J.-W., Song, M.-H., Bediako, J. K., and Yun, Y.-S. (2020). Sequential Recovery of Gold and Copper from Bioleached Wastewater Using Ion Exchange Resins. *Environ. Pollut.* 266, 115167. doi:10.1016/j.envpol.2020.115167

Choudhary, B., and Paul, D. (2018). Isotherms, Kinetics and Thermodynamics of Hexavalent Chromium Removal Using Biochar. *J. Environ. Chem. Eng.* 6, 2335–2343. doi:10.1016/j.jece.2018.03.028

Du, X., Han, Q., Li, J., and Li, H. (2017). The Behavior of Phosphate Adsorption and its Reactions on the Surfaces of Fe-Mn Oxide Adsorbent. *J. Taiwan Inst. Chem. Eng.* 76, 167–175. doi:10.1016/j.jtice.2017.04.023

Du, X., Yu, Z., and Zhu, Y. (2019). Cr(VI) Adsorption from Aqueous Solution and its Reactions Behavior on the Surfaces of Granular Fe-Mn Binary Oxides. *Environ. Prog. Sustain. Energ.* 38, S176–S184. doi:10.1002/ep.12968

Grady, H., and Kenneth, L. (2006). Application of Factorial and Response Surface Methodology in Modern Experimental Design and Optimization. *Crit. Rev. Anal. Chem.* 36, 141–151. doi:10.1080/10408340600969478

Granados-Correa, F., and Bulbulian, S. (2012). Co(II) Adsorption in Aqueous Media by a Synthetic Fe-Mn Binary Oxide Adsorbent. *Water Air Soil Pollut.* 223, 4089–4100. doi:10.1007/s11270-012-1175-8

Guo, J., Yan, C., Luo, Z., Fang, H., Hu, S., and Cao, Y. (2019). Synthesis of a Novel Ternary HA/Fe-Mn Oxides-Loaded Biochar Composite and its Application in Cadmium(II) and Arsenic(V) Adsorption. *J. Environ. Sci.* 85, 168–176. doi:10.1016/j.jes.2019.06.004

Hanrahan, G., and Lu, K. (2006). Application of Factorial and RSM in Modern Experimental Design and Optimization. *Crit. Rev. Anal. Chem.* 36 (3-4), 141–151. doi:10.1080/10408340600969478

He, Y.-Q., and Tan, T.-W. (2006). Use of Response Surface Methodology to Optimize Culture Medium for Production of Lipase with Candida Sp. 99-125. *J. Mol. Catal. B: Enzymatic* 43, 9–14. doi:10.1016/j.molcatb.2006.02.018

Intani, K., Latif, S., Cao, Z., and Müller, J. (2018). Characterisation of Biochar from maize Residues Produced in a Self-Purging Pyrolysis Reactor. *Bioresour. Techn.* 265, 224–235. doi:10.1016/j.biortech.2018.05.103

Jang, J., and Lee, D. S. (2018). Magnetite Nanoparticles Supported on Organically Modified Montmorillonite for Adsorptive Removal of Iodide from Aqueous Solution: Optimization Using Response Surface Methodology. *Sci. Total Environ.* 615, 549–557. doi:10.1016/j.scitotenv.2017.09.324

Kretschmer, I., Senn, A. M., Meichtry, J. M., Custo, G., Halac, E. B., Dillert, R., et al. (2019). Photocatalytic Reduction of Cr(VI) on Hematite Nanoparticles in the Presence of Oxalate and Citrate. *Appl. Catal. B: Environ.* 242, 218–226. doi:10.1016/j.apcatb.2018.09.059

Kuan, D., Dai, L., Liu, D., Du, W., and Liu, H. (2019). A Novel Clean Process for the Combined Production of Fatty Acid Ethyl Esters (FAEEs) and the Ethyl Ester of Polyunsaturated Fatty Acids (PUFAs) from Microalgae Oils. *Renew. Energ.* 143, 772–778. doi:10.1016/j.renene.2019.04.043

Li, L., Lai, C., Huang, F., Cheng, M., Zeng, G., Huang, D., et al. (2019). Degradation of Naphthalene with Magnetic Bio-Char Activate Hydrogen Peroxide: Synergism of Bio-Char and Fe-Mn Binary Oxides. *Water Res.* 160, 238–248. doi:10.1016/j.watres.2019.05.081

Li, L., Pang, H., He, J., and Zhang, J. (2019). Characterization of Phosphorus Species Distribution in Waste Activated Sludge after Anaerobic Digestion and Chemical Precipitation with Fe3+ and Mg2+. *Chem. Eng. J.* 373, 1279–1285. doi:10.1016/j.cej.2019.05.146

Li, R., Wang, J. J., Zhou, B., Awasthi, M. K., Ali, A., Zhang, Z., et al. (2016). Recovery of Phosphate from Aqueous Solution by Magnesium Oxide Decorated Magnetic Biochar and its Potential as Phosphate-Based Fertilizer Substitute. *Bioresour. Techn.* 215, 209–214. doi:10.1016/j.biortech.2016.02.125

Li, Y., Wang, H., Wu, P., Yu, L., Rehman, S., Wang, J., et al. (2020). Bioreduction of Hexavalent Chromium on Goethite in the Presence of *Pseudomonas aeruginosa*. *Environ. Pollut.* 265, 114765. doi:10.1016/j.envpol.2020.114765

Liang, C., Fu, F., and Tang, B. (2021). Mn-incorporated Ferrihydrite for Cr(VI) Immobilization: Adsorption Behavior and the Fate of Cr(VI) during Aging. *J. Hazard. Mater.* 417, 126073. doi:10.1016/j.jhazmat.2021.126073

Liang, J., Li, X., Yu, Z., Zeng, G., Luo, Y., Jiang, L., et al. (2017). Amorphous MnO2 Modified Biochar Derived from Aerobically Composted Swine Manure for Adsorption of Pb(II) and Cd(II). *ACS Sustain. Chem. Eng.* 5, 5049–5058. doi:10.1021/acssuschemeng.7b00434

Liang, M. N., Xu, S. P., Ding, Y. M., and Yan, L. L. (2019). *Preparation Method and Application of mulberry Stem biochar/Fe-Mn Composite Adsorbent*, 5. China: Intellectual Property Office of the People's Republic of China, 07–24.

Liang, M. N., Xu, S. P., Zhu, Y. N., Chen, X., Deng, Z. L., Yan, L. L., et al. (2020). Preparation and Characterization of Fe-Mn Binary Oxide/Mulberry Stem Biochar Composite Adsorbent and Adsorption of Cr(VI) from Aqueous Solution. *Int. J. Env. Res. Pub. He.* 17 (1-16), 676. doi:10.3390/ijerph17030676

Liao, F., Yang, L., Li, Q., Li, Y.-R., Yang, L.-T., Anas, M., et al. (2018). Characteristics and Inorganic N Holding Ability of Biochar Derived from the Pyrolysis of Agricultural and Forestal Residues in the Southern China. *J. Anal. Appl. Pyrolysis* 134, 544–551. doi:10.1016/j.jaap.2018.08.001

Lin, L., Qiu, W., Wang, D., Huang, Q., Song, Z., and Chau, H. W. (2017). Arsenic Removal in Aqueous Solution by a Novel Fe-Mn Modified Biochar Composite: Characterization and Mechanism. *Ecotoxicol. Environ. Saf.* 144, 514–521. doi:10.1016/j.ecoenv.2017.06.063

Liu, J., Cheng, W., Yang, X., and Bao, Y. (2020). Modification of Biochar with Silicon by One-step Sintering and Understanding of Adsorption Mechanism on Copper Ions. *Sci. Total Environ.* 704, 135252. doi:10.1016/j.scitotenv.2019.135252

Liu, X., Pang, H., Liu, X., Li, Q., Zhang, N., Mao, L., et al. (2021). Orderly Porous Covalent Organic Frameworks-Based Materials: Superior Adsorbents for

Pollutants Removal from Aqueous Solutions. *The Innovation* 2 (1), 100076. doi:10.1016/j.xinn.2021.100076

Liu, X., Yang, L., Zhao, H., and Wang, W. (2020). Pyrolytic Production of Zerovalent Iron Nanoparticles Supported on rice Husk-Derived Biochar: Simple, *In Situ* Synthesis and Use for Remediation of Cr(VI)-polluted Soils. *Sci. Total Environ.* 708, 134479. doi:10.1016/j.scitotenv.2019.134479

Luo, C., Tian, Z., Yang, B., Zhang, L., and Yan, S. (2013). Manganese Dioxide/iron Oxide/acid Oxidized Multi-Walled Carbon Nanotube Magnetic Nanocomposite for Enhanced Hexavalent Chromium Removal. *Chem. Eng. J.* 234, 256–265. doi:10.1016/j.cej.2013.08.084

Luo, X., Huang, Z., Lin, J., Li, X., Qiu, J., Liu, J., et al. (2020). Hydrothermal Carbonization of Sewage Sludge and *In-Situ* Preparation of hydrochar/MgAl-Layered Double Hydroxides Composites for Adsorption of Pb(II). *J. Clean. Prod.* 258, 120991. doi:10.1016/j.jclepro.2020.120991

Lv, X., Xu, J., Jiang, G., Tang, J., and Xu, X. (2012). Highly Active Nanoscale Zero-Valent Iron (nZVI)-Fe3O4 Nanocomposites for the Removal of Chromium(VI) from Aqueous Solutions. *J. Colloid Interf. Sci.* 369, 460–469. doi:10.1016/j.jcis.2011.11.049

Lv, Y. Y., Jiang, H. J., Li, S. Y., Han, B., Liu, Y., Yang, D. Q., et al. (2020). Sulforaphane Prevents Chromium-Induced Lung Injury in Rats *via* Activation of the Akt/GSK-3b/Fyn Pathway. *Environ. Pollut.* 259, 113832. doi:10.1016/j.envpol.2019.113812

Ma, H., and Tsai, S.-B. (2017). Design of Research on Performance of a New Iridium Coordination Compound for the Detection of Hg2+. *Ijerph* 14 (10), 1232. doi:10.3390/ijerph14101232

Ma, L., Wang, L., Tang, J., and Yang, Z. (2016). Optimization of Arsenic Extraction in rice Samples by Plackett-Burman Design and Response Surface Methodology. *Food Chem.* 204, 283–288. doi:10.1016/j.foodchem.2016.02.126

Markovski, J. S., Marković, D. D., Đokić, V. R., Mitrić, M., Ristić, M. Đ., Onjia, A. E., et al. (2014). Arsenate Adsorption on Waste Eggshell Modified by Goethite, α-MnO2 and Goethite/α-MnO2. *Chem. Eng. J.* 237, 430–442. doi:10.1016/j.cej.2013.10.031

Mondal, P., Balomajumder, C., and Mohanty, B. (2007). A Laboratory Study for the Treatment of Arsenic, Iron, and Manganese Bearing Ground Water Using Fe^{3+} Impregnated Activated Carbon: Effects of Shaking Time, pH and Temperature. *J. Hazars. Mater.* 144 (1-2), 420–426. doi:10.1016/j.jhazmat.2006.10.078

MourabetRhilassi, M., El Rhilassi, A., El Boujaady, H., Bennani-Ziatni, M., El Hamri, R., and Taitai, A. (2012). Removal of Fluoride from Aqueous Solution by Adsorption on Apatitic Tricalcium Phosphate Using Box-Behnken Design and Desirability Function. *Appl. Surf. Sci.* 258 (10), 4402–4410. doi:10.1016/j.apsusc.2011.12.125

Pap, S., Bezanovic, V., Radonic, J., Babic, A., Saric, S., Adamovic, D., et al. (2018). Synthesis of Highly-Efficient Functionalized Biochars from Fruit Industry Waste Biomass for the Removal of Chromium and lead. *J. Mol. Liquids* 268, 315–325. doi:10.1016/j.molliq.2018.07.072

Park, J. H. (2020). Contrasting Effects of Cr(III) and Cr(VI) on Lettuce Grown in Hydroponics and Soil: Chromium and Manganese Speciation. *Environ. Pollut.* 266, 115073. doi:10.1016/j.envpol.2020.115073

Pei, G., Zhu, Y., Wen, J., Pei, Y., and Li, H. (2020). Vinegar Residue Supported Nanoscale Zero-Valent Iron: Remediation of Hexavalent Chromium in Soil. *Environ. Pollut.* 256, 113407. doi:10.1016/j.envpol.2019.113407

Peng, Y., Sun, Y., Sun, R., Zhou, Y., Tsang, D. C. W., and Chen, Q. (2019). Optimizing the Synthesis of Fe/Al (Hydr)oxides-Biochars to Maximize Phosphate Removal *via* Response Surface Model. *J. Clean. Prod.* 237, 117770. doi:10.1016/j.jclepro.2019.117770

Poguberovi´, S. S., Krčmar, D. M., Maletic´, S. P., Kónya, Z., Pilipovic´, D. D. T., Kerkez, D. V., et al. (2016). Removal of As(III) and Cr(VI) from Aqueous Solutions Using "green" Zero-Valent Iron Nanoparticles Produced by Oak, mulberry and Cherry Leaf Extracts. *Ecol. Eng.* 74 (9), 2115–2123. doi:10.2166/wst.2016.387

Qin, H., Hu, T., Zhai, Y., Lu, N., and Aliyeva, J. (2020). The Improved Methods of Heavy Metals Removal by Biosorbents: A Review. *Environ. Pollut.* 258, 113777. doi:10.1016/j.envpol.2019.113777

Qiu, Y., Zhang, Q., Gao, B., Li, M., Fan, Z., Sang, W., et al. (2020). Removal Mechanisms of Cr(VI) and Cr(III) by Biochar Supported Nanosized Zero-Valent Iron: Synergy of Adsorption, Reduction and Transformation. *Environ. Pollut.* 265, 115018. doi:10.1016/j.envpol.2020.115018

Rogovska, N., Laird, D., Cruse, R. M., Trabue, S., and Heaton, E. (2012). Germination Tests for Assessing Biochar Quality. *J. Environ. Qual.* 41 (4), 1014–1022. doi:10.2134/jeq2011.0103

Senthilkumar, R., Reddy Prasad, D. M., Govindarajan, L., Saravanakumar, K., and Naveen Prasad, B. S. (2019). Synthesis of green marine Algal-Based Biochar for Remediation of Arsenic(V) from Contaminated Waters in Batch and Column Mode of Operation. *Int. J. Phytoremediat.* 22 (3), 279–286. doi:10.1080/15226514.2019.1658710

Tang, J., Zhao, B., Lyu, H., and Li, D. (2021). Development of a Novel Pyrite/biochar Composite (BM-FeS2@BC) by ball Milling for Aqueous Cr(VI) Removal and its Mechanisms. *J. Hazard. Mater.* 413, 125415. doi:10.1016/j.jhazmat.2021.125415

Tang, T., Liu, X., Wang, L., Zuh, A. A., Qiao, W., and Huang, J. (2020). Uptake, Translocation and Toxicity of Chlorinated Polyfluoroalkyl Ether Potassium Sulfonate (F53B) and Chromium Co-contamination in Water Spinach (Ipomoea Aquatica Forsk). *Environ. Pollut.* 266, 115385. doi:10.1016/j.envpol.2020.115385

Vasiee, A., Behbahani, B. A., Yazdi, F. T., and Moradi, S. (2016). Optimization of the Production Conditions of the Lipase Produced by Bacillus Cereus from rice Flour through Plackett-Burman Design (PBD) and Response Surface Methodology (RSM). *Microb. Pathogenesis* 101, 36–43. doi:10.1016/j.micpath.2016.10.020

Wang, H., Guo, H., Zhang, N., Chen, Z., Hu, B., and Wang, X. (2019). Enhanced Photoreduction of U(VI) on C3N4 by Cr(VI) and Bisphenol A: ESR, XPS, and EXAFS Investigation. *Environ. Sci. Technol.* 53, 6454–6461. doi:10.1021/acs.est.8b06913

Wang, J., and Wang, S. (2019). Preparation, Modification and Environmental Application of Biochar: A Review. *J. Clean. Prod.* 227, 1002–1022. doi:10.1016/j.jclepro.2019.04.282

Wang, W. L., and Fu, X. B. (2013). Efficient Removal of Cr(VI) with Fe/Mn Mixed Metal Oxide Nanocomposites Synthesized by a Grinding Method. *J. Nanomater.* 514917, 1–8.

Wang, X. X., Li, X., Wang, J. Q., and Zhu, H. T. (2020). Recent Advances in Carbon Nitride-Based Nanomaterials for the Removal of Heavy Metal Ions from Aqueous Solution. *J. Inorg. Mater.* 35, 260–270. doi:10.15541/jim20190436

Wen, X., Sun, N., Yan, C., Zhou, S., and Pang, T. (2018). Rapid Removal of Cr(VI) Ions by Densely Grafted Corn Stalk Fibers: High Adsorption Capacity and Excellent Recyclable Property. *J. Taiwan Inst. Chem. Eng.* 89, 95–104. doi:10.1016/j.jtice.2018.04.021

Wen, Z., Zhang, Y., Guo, S., and Chen, R. (2017). Facile Template-free Fabrication of Iron Manganese Bimetal Oxides Nanospheres with Excellent Capability for Heavy Metals Removal. *J. Colloid Interf. Sci.* 486, 211–218. doi:10.1016/j.jcis.2016.09.026

Xiong, Y., Tong, Q., Shan, W., Xing, Z., Wang, Y., Wen, S., et al. (2017). Arsenic Transformation and Adsorption by Iron Hydroxide/manganese Dioxide Doped Straw Activated Carbon. *Appl. Surf. Sci.* 416, 618–627. doi:10.1016/j.apsusc.2017.04.145

Xu, Z., Xu, X., Yu, Y., Yao, C., Tsang, D. C. W., and Cao, X. (2021). Evolution of Redox Activity of Biochar during Interaction with Soil Minerals: Effect on the Electron Donating and Mediating Capacities for Cr(VI) Reduction. *J. Hazard. Mater.* 414, 125483. doi:10.1016/j.jhazmat.2021.125483

Yacou, C., Altenor, S., Carene, B., and Gaspard, S. (2018). Chemical Structure Investigation of Tropical Turbinaria Turbinata Seaweeds and its Derived Carbon Sorbents Applied for the Removal of Hexavalent Chromium in Water. *Algal. Res.* 34, 25–36. doi:10.1016/j.algal.2018.06.014

Ye, G., Yu, Z., Li, Y., Li, L., Song, L., Gu, L., et al. (2019). Efficient Treatment of Brine Wastewater through a Flow-Through Technology Integrating Desalination and Photocatalysis. *Water Res.* 157, 134–144. doi:10.1016/j.watres.2019.03.058

Yu, Y., An, Q., Jin, L., Luo, N., Li, Z., and Jiang, J. (2020). Unraveling Sorption of Cr (VI) from Aqueous Solution by FeCl3 and ZnCl2-Modified Corn Stalks Biochar: Implicit Mechanism and Application. *Bioresour. Techn.* 297, 122466. doi:10.1016/j.biortech.2019.122466

Zhang, X., Fu, W., Yin, Y., Chen, Z., Qiu, R., Simonnot, M.-O., et al. (2018). Adsorption-reduction Removal of Cr(VI) by Tobacco Petiole Pyrolytic Biochar: Batch experiment, Kinetic and Mechanism Studies. *Bioresour. Techn.* 268, 149–157. doi:10.1016/j.biortech.2018.07.125

Zhang, X., Zang, C., Ma, H. L., and Wang, Z. J. (2020). Study on Removing Calcium Carbonate Plug from Near Wellbore by High-Power Ultrasonic Treatment. *ULTRASON. SONOCHEM.* 62 (03), 006. doi:10.1016/j.ultsonch.2019.03.006

Zhao, Y., Kang, D. J., Chen, Z., Zhan, J. J., and Wu, X. Q. (2018). Removal of Chromium Using Electrochemical Approaches: A Review. *Int. J. Electrochem. Sci.* 13, 1250–1259. doi:10.20964/2018.02.46

Zhong, X., Lu, Z., Liang, W., and Hu, B. (2020). The Magnetic Covalent Organic Framework as a Platform for High-Performance Extraction of Cr(VI) and Bisphenol a from Aqueous Solution. *J. Hazard. Mater.* 393, 122353. doi:10.1016/j.jhazmat.2020.122353

Zhou, L., Liu, Y., Liu, S., Yin, Y., Zeng, G., Tan, X., et al. (2016). Investigation of the Adsorption-Reduction Mechanisms of Hexavalent Chromium by Ramie Biochars of Different Pyrolytic Temperatures. *Bioresour. Techn.* 218, 351–359. doi:10.1016/j.biortech.2016.06.102

Conflict of Interest: The authors declare that the research was conducted in the absence of any commercial or financial relationships that could be construed as a potential conflict of interest.

Publisher's Note: All claims expressed in this article are solely those of the authors and do not necessarily represent those of their affiliated organizations, or those of the publisher, the editors and the reviewers. Any product that may be evaluated in this article, or claim that may be made by its manufacturer, is not guaranteed or endorsed by the publisher.